Study of the mechanism of the vanadium 4+/5+ redox reaction in acidic solutions

Gattrell, M.; Park, J.; MacDougall, B.; Apte, J.; McCarthy, S.; Wu, C. W.

Publisher's version / Version de l'éditeur:
https://doi.org/10.1149/1.1630594
Journal of the Electrochemical Society, 151, 1, pp. A123-A130, 2004

Journal of The Electrochemical Society, **151** (1) A123-A130 (2004)
0013-4651/2003/151(1)/A123/8/$7.00 © The Electrochemical Society, Inc.

Study of the Mechanism of the Vanadium 4+/5+ Redox Reaction in Acidic Solutions

M. Gattrell,[a,*,z] J. Park,[a] B. MacDougall,[a,*] J. Apte,[b] S. McCarthy,[c] and C. W. Wu[c]

[a]*Institute for Chemical Process and Environmental Technology, National Research Council of Canada, Ottawa, Ontario K1A 0R6, Canada*
[b]*McGill University, Montreal, Quebec, Canada*
[c]*University of Waterloo, Waterloo, Ontario, Canada*

The mechanism of the vanadium VO^{2+}/VO_2^+ redox couple has been examined in acidic aqueous solutions. A detailed understanding of this chemistry is of interest for improving and optimizing the performance of vanadium redox-flow batteries, a promising electrochemical electricity storage technology. The vanadium 4+/5+ redox reactions were studied at a rotating disk graphite electrode and polarization curves were obtained in sulfuric acid and perchloric acid, with varying pH and vanadium concentrations. The results were compared to model predictions for different mechanisms. The data were consistent with a model with a multistep chemical-electrochemical-chemical mechanism at low overpotentials, which changes to a multistep electrochemical-chemical-chemical mechanism at higher anodic or cathodic overpotentials. Unusually high Tafel slopes (350-450 mV/decade) were observed for the reduction of VO_2^+ at higher overpotentials. While this could not be directly explained by the model, insights gained through the use of the model can provide the basis for some suggestions.
 [DOI: 10.1149/1.1630594]

Manuscript received March 27, 2003. Available electronically December 9, 2003.

A more detailed understanding of vanadium redox chemistry is of interest because of its application in vanadium-based redox flow batteries. Redox flow batteries are an electrochemical energy storage technology where the energy, rather than being stored at the electrodes like batteries, is stored by chemical changes to species dissolved in a working fluid. Various systems based on different species have been proposed over the years with two presently being commercialized. One system is based on S/S^{-2} and Br^-/Br_3^{-1} and the other based on V^{2+}/V^{3+} and VO^{2+}/VO_2^+.[2] While the polysulphide/bromine system has a higher cell voltage (*ca.* 1.52 V), the vanadium-based system (*ca.* 1.40 V) is simpler and more rugged, in part because it is less affected by membrane crossover problems. Thus, the vanadium system has an advantage for remote or unattended operation.

Figure 1 shows the main components of a vanadium redox-flow battery (VRB) system. The electrochemical cell stores or releases power by shifting the ratio of the two vanadium species present at each electrode. The system power is determined by the rate of reaction of the vanadium species at each electrode and the total surface area of the electrodes. The amount of energy stored in the system is determined by the concentration of the vanadium species and the volume of the reservoirs.

Because the solubility of the redox species in the working fluid is limited, the volumetric and specific energy densities are low. Therefore, the development of these systems has focused on stationary applications. The cost of a system will increase with the power output of the system based on the cost of the electrochemical cell, and the cost will increase with the energy storage capacity of the system based on the (typically lower) cost of the reservoirs and the vanadium solution. Thus, redox flow-type batteries are particularly suited for longer-term energy storage.

As well as applications such as load levelling and reliable power, redox flow batteries seem well suited for storing electricity produced by intermittent renewable energy sources such as wind or solar power. Present systems typically use lead acid batteries. Because lead acid batteries store energy in a coating on the electrode plates, the system energy storage and power output are both related to the electrode area. For lead acid batteries this makes increased energy storage (and so increased capture of wind or solar energy) proportionally more expensive, a fact that limits the most cost efficient size of the renewable energy storage.[3] It is hoped that the different cost relationships of the vanadium redox batteries will improve this situation. A further advantage is the much higher cycle life and simple cycling considerations for redox flow batteries, because the active materials are kept in solution and are not lost nor degraded by battery cycling. Thus this relatively new electrochemical technology seems well suited for enhancing the utilization of renewable energy.[4-7] It has also been reported that the life cycle environmental impact of using VRBs is lower than that for lead acid battery power storage systems.[8]

The typical electrodes are carbon based because of their wide operating potential range (minimal hydrogen and oxygen evolution), stability as both an anode and a cathode, and availability in high surface area at reasonable cost. Carbon has a very wide range of characteristics depending on the methods of manufacturing and preparation. Commercial vanadium battery electrodes typically use carbon felt, made by pyrolysis of polymers (either rayon or polyacrylonitrile based[9]), which can be treated to increase the number of surface oxide sites,[10,11] or heated to increase its crystallinity and conductivity.[12] The electrolyte usually has from 1 to 3 M of vanadium sulfates in 1 to 2 M H_2SO_4.

The reactions occurring at both electrodes during discharging of the VRB are typically written as shown below

$$V^{2+} \rightleftarrows V^{3+} + e- \quad [1]$$

$$VO_2^+ + e- + 2H^+ \rightleftarrows VO^{2+} + H_2O \quad [2]$$

The standard potential for Reaction 1 is reported to be −0.255 V *vs.* normal hydrogen electrode (NHE)[13,14] However, standard potentials of −0.258 and −0.291 V have been reported based on measurements in 0.5 and 3 M H_2SO_4 solutions, respectively.[13] For Reaction 2, the standard potential is reported as 1.000[13] or 1.004 V[14] with values of 1.008 and 1.103 V reported based on measurements in 1 and 3 M H_2SO_4 solutions, respectively.[13] Thus, for VRB cells, the open circuit cell voltage at 50% state of charge is often found to be higher than the theoretical value of about 1.257 V due to the high concentrations of sulphuric acid and vanadium sulfates used.

The redox reaction of the VO^{2+}/VO_2^+ couple in acid has been studied on platinum, but the data is complicated because the degree of surface oxide coverage of the platinum electrodes strongly influenced the results.[13] Reduction of 1 mM VO_2^+ on graphite in a mix of 1 M H_2SO_4 and 1 M H_3PO_4 has been reported to be irreversible and result in a double wave.[15] The reaction has recently been more actively studied as part of its development as a candidate for redox

* Electrochemical Society Active Member.
z E-mail: michael.gattrell@nrc-cnrc.gc.ca

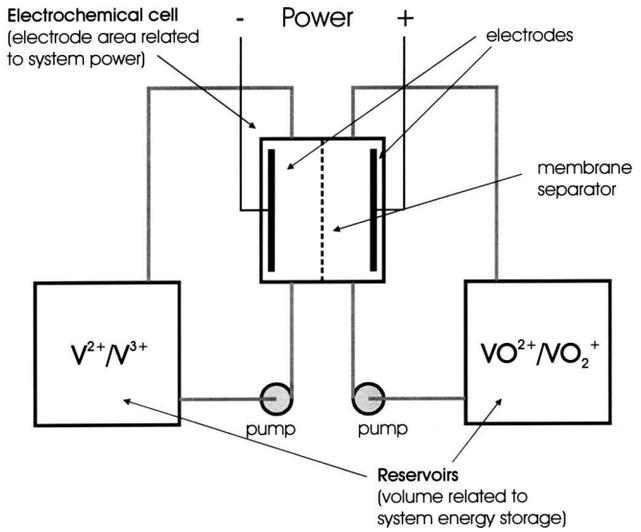

Figure 1. VRB system with electrodes, membrane separator, pumps, and reservoirs.

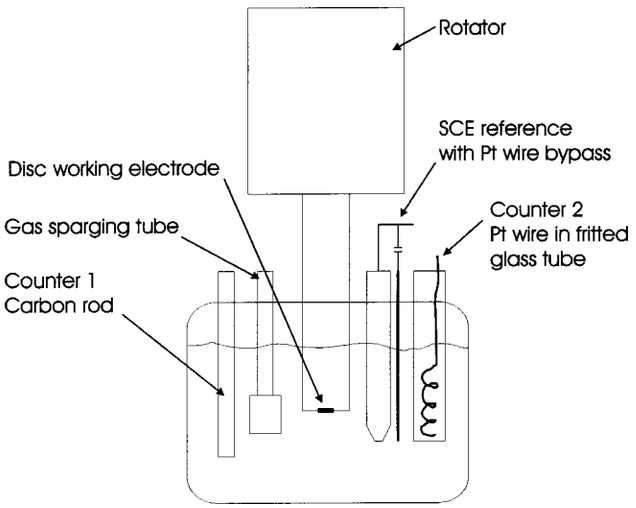

Figure 2. The experimental setup. A sealed, water-jacketed RDE cell, with a removable second counter electrode compartment for preparing oxidized or reduced solutions.

energy storage.[16,17] In this work, the reactions were studied using cyclic voltammetry, and some polarization curves were measured at a rotating disk electrode (RDE). In the latter tests, the oxidation of VO^{2+} appeared to be straightforward and amenable to standard electrochemical measurement approaches, but the reduction of VO_2^+ did not yield an easily interpreted polarization curve.[17] In earlier work, we also have found that the polarization curves for the VO^{2+}/VO_2^+ redox reactions cannot be fit using a simple Butler-Volmer kinetic equation.[18] In this work we therefore attempt to study in more detail the mechanism of Reaction 2, which can be seen from its equation to be a multistep reaction.

Experimental

The rotating disk system, including glassy carbon (GC) and graphite disc electrodes (0.196 cm^2), an AFMSRX electrode rotator, and the RDE cell (modified with a water jacket) was obtained from Pine Instruments. An EG&G 263 potentiostat was used with Scribner CorrWare and CorrView 2.3f data collection and analysis software. For most of the work, a cracked bead low flow junction standard calomel electrode (SCE) reference (Fisher Scientific Accumet, <5 uL/h flow rate) was used to minimize possible solution contamination over long run times. A platinum wire pseudo-reference was used in parallel, connected via a series 10 μF capacitor, in order to decrease the reference electrode impedance and improve the potentiostat stability.[19] A carbon rod counter electrode was used during experimental measurements, while a platinum wire counter electrode in a separate compartment was used (with the carbon rod as the working electrode) to prepare oxidized or reduced solutions (see diagram in Fig. 2). This allowed oxidized (VO_2^+) or reduced solutions (V^{2+} or V^{3+}) to be prepared.

The chemicals used include $VOSO_4$ from Alfa Aesar (with certificates of analysis showing 99.9+% on a metals basis), ACS grade H_2SO_4, $HClO_4$, and Na_2CO_3 from EM Science, and deionized water from a Millipore Milly-Q Plus system.

The electrodes were initially hand polished with 600 and 1200 grit paper, then polished with a Buehler polisher at 100 rpm using Nanocloth with 1, 0.3, and 0.05 μm alumina, followed by a thorough rinsing on the wheel. Some tests were done where the electrode was placed in an ultrasonic bath for periods from 5 to 15 min, which resulted in a slightly lower activity, but the same shape of polarization curve (*i.e.*, a slightly lower k^0). Thereafter, between experiments, a simple polish with 0.05 μm alumina and a thorough rinsing on the wheel was used. It should be noted that other workers have found that the activity of the electrodes can be increased through more complex polishing methods.[20] However, it was the intent of this paper to study the influence of the solution chemistry on the reaction, and so our goal was simply to prepare a reproducible surface.

Removing dissolved oxygen by sparging the solutions with argon was observed to have no effect on the VO^{2+}/VO_2^+ couple, though it was of course required to obtain the V^{2+}/V^{3+} couple. Because of possible contamination from the SCE electrode, a test was carried out where chloride was added to the cell, which resulted in no significant change to the voltammetry.

The concentrations of the vanadium species were measured from the limiting currents at various RDE rotation rates. Unfortunately, no clear limiting current plateau was observed for the reduction of VO_2^+ prior to the onset of other possible reactions such as VO^{2+} to V^{3+} (E° = 0.377 V *vs.* standard hydrogen electrode, SHE) or to V^{2+} (E° = −0.255 V *vs.* SHE)[14] (see Fig. 3). However, known solutions of $VOSO_4$ could be used to estimate the diffusion coefficient for VO^{2+}. The value obtained in 1 M H_2SO_4 was 3.0 ± 0.3 × 10^{-6} cm^2/s (calculated using a density of 1.066 g/cm^3 and viscosity of 1.23 g/cms[21]). The high degree of uncertainty is due to the high oxygen evolution background (as can be seen by the sloped limiting current plateaus in Fig. 3). Following this, mixtures of VO^{2+} and VO_2^+ were produced by galvanostatic oxidation using a cathode in a separate compartment (as described above). The concentration of VO^{2+} in the test mixture could then be determined using the limiting current for VO^{2+} oxidation. The VO_2^+ was then found by difference from the known starting total vanadium concentration. The open circuit potential was also used as a check on the solution composition, but due to the slow kinetics for the VO^{2+}/VO_2^+ system, it was not as reliable. For the V^{2+}/V^{3+} system the ability to clearly measure both limiting current plateaus, plus knowing the total vanadium concentration, can provide a method for determining the diffusion coefficients in the solution of interest and thus checking solution compositions.

Note also that the choice of sweep rates for the various measurements was typically a compromise. In order obtain steady-state data, a slow sweep rate is desirable. However, too great a combination of anodic potential and time leads to oxidation of the carbon surface and a resulting loss in electrode activity (attributed to the formation of a multilayer oxide film[22]). For measuring the limiting current plateau, which required fairly anodic potentials to reach the mass transfer limited region, sweep rates around 10 to 30 mV/s were

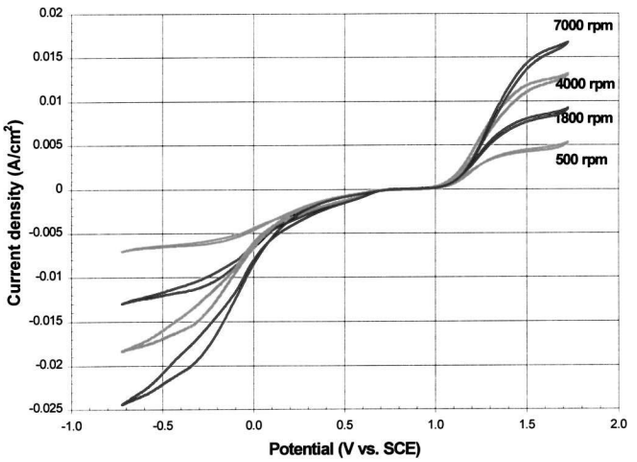

Figure 3. RDE polarization curves at various rotation rates. Graphite electrode, 1 M H_2SO_4, 21 mM V(IV), and 29 mM V(V).

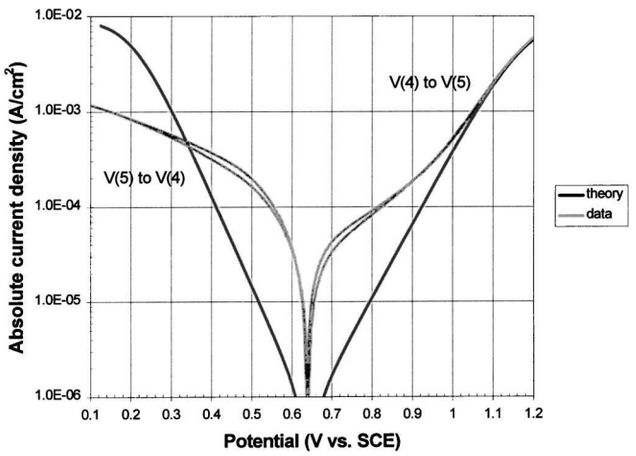

Figure 5. Polarization curve for the graphite electrode. Sweep rate 0.1 mV/s, 20°C, 4000 rpm, approximately 90 mM VO^{2+} and 110 mM VO_2^+, 1 M H_2SO_4. Theoretical lines based on $k_0 = 3.0 \times 10^{-7}$ cm/s, $E^0 = 0.785$ V, and Tafel slope for VO^{2+} to VO_2^+ of 138 mV/decade.

used. For measuring the polarization curves a lower anodic limit was used and so sweep rates from 0.1 to 1 mV/s were used. Even so, in some experiments, hysterisis and a slow drift in activity with sweep number was noted. Because of this, for most of the results that follow, both the forward and reverse sweeps are shown.

Results and Discussion

Typical polarization curves measured at the RDE are shown in Fig. 4 and provide a good overview of the redox battery reactions. The reversible potentials (*i.e.*, corrected to equimolar concentrations) are located at −0.50 and 0.76 V, giving a difference of about 1.26 V. It can also be seen that the kinetics of the VO^{2+}/VO_2^+ couple were slower than the V^+/V^{2+} couple.

A Tafel type plot of the polarization curve for the VO^{2+}/VO_2^+ reaction is shown in Fig. 5. Also plotted is the calculated response expected for a simple electrochemical system. This calculation used the Butler-Volmer equation with a formal potential of $E^0 = 0.781$ V (estimated from the zero crossing point of the curves and the vanadium species' concentrations), and a standard rate constant of $k_0 = 3.0 \times 10^{-7}$ cm/s with a Tafel slope for VO^{2+} to VO_2^+ of 138 mV/decade equal to a transfer coefficient (α) of 0.42 (taken from the straight line region from about 1.0 to 1.175 V). It can be seen from Fig. 5 that there are significant deviations from a simple mechanism. A shoulder is apparent on the anodic Tafel slope from 0.785 to 0.95 V, and possibly a similar shoulder from 0.785 to 0.6 V on the cathodic side. Also the linear part of the negative going polarization curve (from 0.35 to 0.6 V) has a slope corresponding to $\alpha = 0.15$ (385 mV/decade). Even if the diffusion coefficient for VO_2^+ was as low as 2.0×10^{-6} cm²/s, the expected limiting current for its reduction would be about 0.1 A/cm², and so the high Tafel slope was not due to mass transport limitations. This is also supported by Fig. 3, where the curves for VO_2^+ reduction only show divergence with rotation rate at potentials below about 0.2 V.

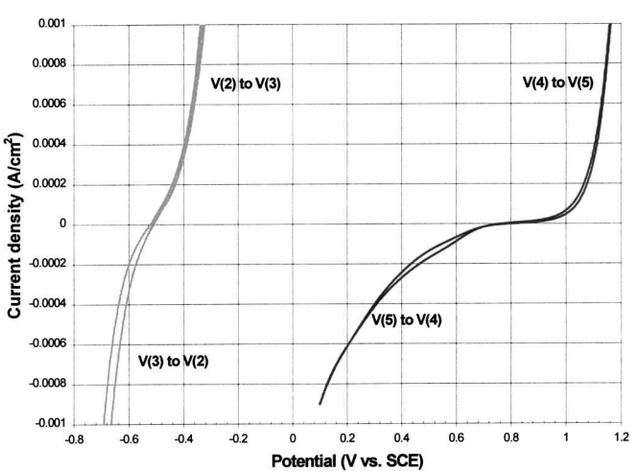

Figure 4. Graphite RDE, 4000 rpm, 0.1 mV/s, 1 M H_2SO_4, 20 C. For V(II)/V(III), *ca.* 16 and 36 mM V^{3+}. For V(IV)/V(V), 31 mM VO^{2+}, and 19 mM VO_2^+.

While these shoulders occur at low current densities (they are barely noticeable on linear plots) they are of interest because the typical real current densities in operating VRBs are very small. While high current density operation can be sustained if demanded by a load, a typical operating target for energy storage is an overall efficiency of around 80%.[23] This would correspond to 90% energy conversion efficiency and hence a maximum cell overvoltage of 0.126 V during the charge and discharge steps. As this total must include the polarization overpotentials of both electrodes and the resistive drop of the cell membrane, one can see that the initial parts of the polarization curve are of significant interest. (One can also understand the interest in specially prepared, high surface area carbon felt electrodes[10-12] to get useful membrane current densities in commercial units.)

The shoulder on the anodic side of the curves increased slightly with electrode cycling, to increase linearly with vanadium concentration, to not increase with rotation rate, and to increase roughly with the square root of sweep rate (after background correcting for the carbon electrode alone). If the shoulder was due to the mass transfer limited reaction of a solution impurity, it would be expected to change with rotation rate. If it was due to a surface bound species it would be expected to increase linearly with sweep rate. It was therefore decided to examine possible mechanisms for the VO^{2+}/VO_2^+ couple, to see what they might predict.

Expected mechanism and model.—The VO^{2+} ion is reported to exist in noncomplexing acidic solutions as the blue oxovanadium ion $[VO(H_2O)_5]^{2+}$.[24] The complex is described as a tetragonal bipyramid (see Fig. 6) with four equatorial waters having residence times of 1.35×10^{-3} s and the axial water being more weakly held with a residence time of 10^{-11} s.[25] In strong acid, VO_2^+ exists as the yellow dioxovanadium ion, *cis*-$[VO_2(H_2O)_4]^+$,[24,25] which has also been drawn in Fig. 6. It should be noted that, at the high vanadium

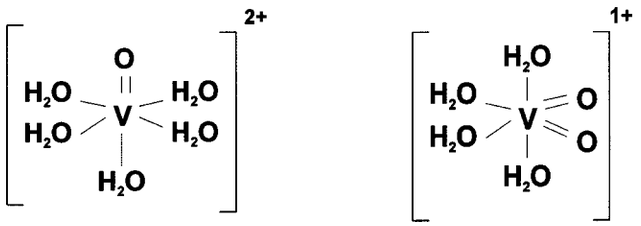

Figure 6. Structures for VO^{2+} and VO_2^+ in noncomplexing acidic solutions (based on Ref. 24 and 25).

and sulfuric acid concentrations encountered in commercial batteries, more complex species have been reported, including $V_2O_3^{3+}$[26] and complexes with sulfate and bisulfate.[27-29] However, for this work, lower concentrations were used, and because it is hoped to obtain an initial basic understanding of the reaction mechanisms, only the aqua complexes were considered.

The overall reaction as written in Eq. 2 would be expected to consist of three elementary steps: one electron transfer and two proton transfers. Using the structures for the ions in noncomplexing acidic solutions, a schematic of the possible mechanism can be written based on various combinations of electron and proton transfers (shown in Fig. 7). It is interesting to note that, while the starting and final vanadium species are the most stable forms around pH 0, the intermediates would only be expected to predominate at higher or lower pH values. The existence of VO^{3+} has been suggested from the variation of the equilibrium potentials of V(IV)/V(V) mixtures in strong acid.[13] It is also unclear what would be the form of VO_2. The hydrated form of VO_2 is usually written as $VO(OH)_2$ and the dry oxide as V_2O_4.[25,14] A simpler version of this mechanism has also been proposed by other workers.[30]

Three different reaction pathways are possible. However, because no transfer coefficients greater than 0.5 were observed, one can conclude that on the dominant pathway the rate determining step cannot come after the electron transfer step. For the cases where a chemical step proceeding the electrochemical step is rate determining, the rate expression used is that suggested for the case where the equilibrium of the chemical step favors the starting compound (A in Eq. 3) (*i.e.*, $K_{eq} = k_f/k_r \ll 1$).[31,32] This assumes that the reaction is governed by the rate of conversion of the starting compound in a depleted zone near the electrode surface

$$\mathrm{A} \underset{k_r}{\overset{k_f}{\rightleftarrows}} \mathrm{B} \underset{-e}{\overset{+e}{\rightleftarrows}} \mathrm{C} \qquad [3]$$

$$i = FD^{1/2}[\mathrm{A}](k_f K_{eq})^{1/2} = Fk_f[\mathrm{A}](DK_{eq}/k_f)^{1/2} \qquad [4]$$

Equation 4 also assumes that the diffusion coefficients of the reacting species are equal (*i.e.*, $D_A = D_B = D$). Then $(DK_{eq}/k_f)^{1/2}$ is the estimate of the thickness of the zone near the electrode surface where the intermediate (B) has been depleted and is being replaced by the reaction of the starting compound (A).

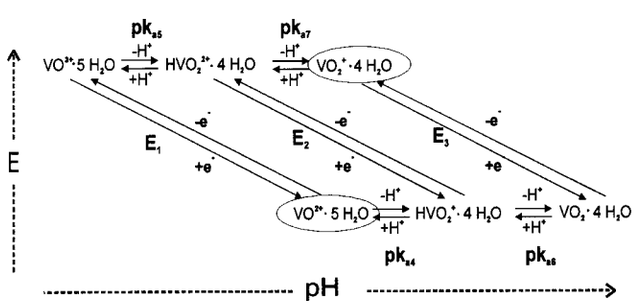

Figure 7. Schematic of the possible reaction pathways between VO^{2+} and VO_2^+ with the individual steps labeled.

Thus reaction rates can be calculated for each possible rate determining step. These calculated rates were then combined to give a model for the overall system. For steps in series, the slowest calculated rate would limit the rate for that pathway. To allow the model to shift smoothly between changing rate determining steps, the expressions for the different possible rate determining steps were added as conductors in series

$$rate_{\mathrm{path1,total}} = 1/(1/rate_{\mathrm{path1,step1}} + 1/rate_{\mathrm{path1,step2}}) \qquad [5]$$

The overall reaction rate was then estimated as the sum of the different parallel pathways. That did not allow for depletion of the concentrations of intermediates shared by two pathways, but was felt to be sufficiently complex to compare against measured data to determine the key rate determining step or steps.

For the purposes of these calculations the forward reaction direction is taken to be the oxidation of VO^{2+} (cell charging). Then each pathway can be written in terms of chemical (C) and electrochemical (E) steps as follows (where the rate determining step is underlined for each case).

Path 1 (ECC).—The rate is given by

$$\underline{\mathrm{E}}\mathrm{CC}: \quad \mathrm{rate} = [VO^{2+}]k_{1f} - [VO^{3+}]k_{1r}$$
$$= [VO^{2+}]k_1^0 \exp[(1-\alpha_1)F(E-E_1^0)/RT] - [[VO_2^+][H^+]^2/(K_{5eq}K_{7eq})]k_1^0 \times \exp[-\alpha_1 F(E-E_1^0)/RT] \qquad [6]$$

Path 2 (CEC).—The rates for the individual steps in Eq. 5 are

$$\underline{\mathrm{C}}\mathrm{EC}: \quad \mathrm{rate} = [VO^{2+}]k_{4f}(D/[H^+]k_{4r})^{1/2} \qquad [7]$$

$$\mathrm{C}\underline{\mathrm{E}}\mathrm{C}: \quad \mathrm{rate} = [HVO_2^+]k_{2f} - [HVO_2^{2+}]k_{2r}$$
$$= ([VO^{2+}]K_{4eq}/[H^+])k_2^0 \exp[(1-\alpha_2) \times F(E-E_2^0)/RT] - ([VO_2^+] \times [H^+]/K_{7eq})k_2^0 \exp[-\alpha_2 F(E-E_2^0)/RT] \qquad [8]$$

Path 3 (CCE).—The rates for the individual steps in Eq. 5 are

$$\underline{\mathrm{C}}\mathrm{CE}: \quad \mathrm{rate} = [VO^{2+}]k_{4f}(D/[H^+]k_{4r})^{1/2} \qquad [9]$$

$$\mathrm{C}\underline{\mathrm{C}}\mathrm{E}: \quad \mathrm{rate} = [HVO_2^+]k_{6f}(D/[H^+]k_{6r})^{1/2}$$
$$= ([VO^{2+}]K_{4eq}/[H^+])k_{6f}(D/[H^+]k_{6r})^{1/2} \qquad [10]$$

$$\mathrm{CC}\underline{\mathrm{E}}: \quad \mathrm{rate} = [VO_2]k_{3f} - [VO_2^+]k_{3r}$$
$$= ([VO^{2+}]K_{4eq}K_{6eq}/[H^+]^2)k_3^0 \exp[(1-\alpha_3) \times F(E-E_3^0)/RT] - [VO_2^+]k_3^0 \times \exp[-\alpha_3 F(E-E_3^0)/RT] \qquad [11]$$

Similarly, for the reverse reaction of the reduction of VO_2^+ (cell discharging), the equations would be

Path 1 (CCE).—The rates for the individual steps in Eq. 5 are

$$\underline{\mathrm{C}}\mathrm{CE}: \quad \mathrm{rate} = [VO_2^+][H^+]k_{7r}(D/k_{7f})^{1/2} \qquad [12]$$

$$\mathrm{C}\underline{\mathrm{C}}\mathrm{E}: \quad \mathrm{rate} = [HVO_2^{2+}][H^+]k_{5r}(D/k_{5f})^{1/2}$$
$$= ([VO_2^+][H^+]^2/K_{7eq})k_{5r}(D/k_{5f})^{1/2} \qquad [13]$$

$$\text{CCE: rate} = [VO^{3+}]k_{1r} - [VO^{2+}]k_{1f}$$
$$= [[VO_2^+][H^+]^2/(K_{5eq}K_{7eq})]k_1^0 \times \exp[-\alpha_1 F(E - E_1^0)/RT] - [VO^{2+}]k_1^0 \times \exp[(1 - \alpha_1)F(E - E_1^0)/RT] \quad [14]$$

Path 2 (CEC).—The rates for the individual steps in Eq. 5 are

$$\text{CEC: rate} = [VO_2^+][H^+]k_{7r}(D/k_{7f})^{1/2} \quad [15]$$

$$\text{CEC: rate} = [HVO_2^{2+}]k_{2r} - [HVO_2^+]k_{2f}$$
$$= ([VO_2^+][H^+]/K_{7eq})k_2^0 \exp[-\alpha_2 F(E - E_2^0)/RT] - ([VO^{2+}]K_{4eq}/[H^+])k_2^0 \exp[(1 - \alpha_2) \times F(E - E_2^0)/RT] \quad [16]$$

Path 3 (ECC).—The rate is given by

$$\text{ECC: rate} = [VO_2^+]k_{3r} - [VO_2]k_{3f}$$
$$= [VO_2^+]k_3^0 \exp(-\alpha_3 F(E - E_3^0)/RT) - ([VO^{2+}]K_{4eq}K_{6eq}/[H^+]^2)k_3^0 \times \exp[(1 - \alpha_3)F(E - E_3^0)/RT] \quad [17]$$

For each chemical step there are two unknowns (k_f and k_r). However, for reaction step 4, the equilibrium is reported in the literature ($pK_{a4} = 5.36$[14]), eliminating one unknown. Also, for each path the overall free energy changes must be the same. Therefore each E^0 can be specified in terms of an overall E^0 as shown below

$$nFE^0_{overall} = nFE_1^0 - RT\ln(K_{5eq}K_{7eq}) \quad [18]$$

$$nFE^0_{overall} = nFE_2^0 - RT\ln(K_{4eq}K_{7eq}) \quad [19]$$

$$nFE^0_{overall} = nFE_3^0 - RT\ln(K_{4eq}K_{6eq}) \quad [20]$$

The model was then tested to see how well it could fit data measured with different vanadium concentrations, pHs, electrolytes, and electrode materials. To further reduce the number of adjustable parameters and because the goal was simply to see the quality of the qualitative fit to the data, values for the various pK_as were arbitrarily set ($pK_{a5} = -3$, $pK_{a6} = 5.6$, and $pK_{a7} = -2$) and the literature value of $E^0_{overall} = 1.004$ V *vs.* SCE[14] was used.

Comparison to data at various pH values and concentrations.—A fit of the model to a polarization curve is shown in Fig. 8A, with a breakdown of the model prediction into its various components shown in Fig. 8B. It can be seen that, except for the region below 0.4 V, the model fit the data quite well. Figure 8B shows how each of the three possible reaction pathways contributed to the overall fit. Near the reversible potential, reaction pathway 2 (CEC) dominated. In that region, the fit was adjusted through [H+] value and k_2^0 (there is insufficient data to adjust α_2 so it was left at 0.5), and the shoulders were then fit by adjusting the associated chemical rate determining steps through k_{4f} and k_{7r}. As the potential became more anodic, reaction pathway 1 (ECC) took over (which was fit using k_1^0 and α_1). Similarly, for the reduction reaction, at more cathodic potentials reaction pathway 3 (ECC) might dominate (which would be fitted using k_3^0 and α_3, though this is not possible because the model did not fit well in this region, as will be discussed later). Thus rather than one mechanism dominating, this would appear to suggest that the preferred mechanistic pathway changes with potential.

One way to test this idea is by varying the solution pH, because the different reaction pathways are expected to have different pH dependencies. At the extreme potentials, oxidation of VO^{2+} to VO_2^+ via path 1 (ECC) and reduction of VO_2^+ to VO^{2+} via path 3 (ECC), would both be expected to be pH independent. The reversible potential will be dependent on the square of pH, while the shoulder regions, being limited by potential independent acid-base reaction steps [(CEC) pathways], would vary linearly with pH. This is best tested using a perchloric acid electrolyte, because of its simpler acid-base chemistry.

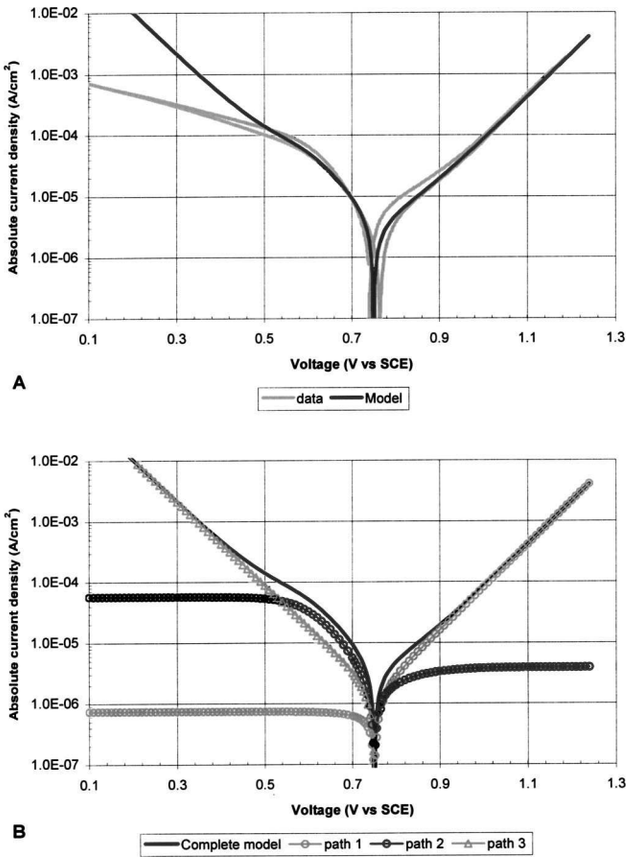

Figure 8. (A) The model fitted to a set of data. (B) The contribution of the various reaction pathways to the complete model fit. Data measured at a graphite electrode, 4000 rpm, 33 mM V(IV), and 17 mM V(V), 1.9 M H_2SO_4 + 1.4 M $KHCO_3$.

The effect of pH on the polarization curves is shown in Fig. 9A for a 2 M $HClO_4$ solution that was neutralized stepwise with $NaHCO_3$. As the pH increased, the reversible potential moved to more cathodic potentials. However, the anodic linear Tafel regions (from about 1.3 to 1.5 V) remain roughly the same and so the shoulder region anodic to the reversible potential becomes more pronounced. The cathodic region also shows little pH dependence below 0.5 V. This is consistent with the idea that the preferred mechanistic pathway changes with potential. In Fig. 9B the model predictions are shown. The model was fitted to the data for pH −0.04, then the various constants were kept fixed and changing the $[H^+]$ value was used to match the reversible potential of the model with the data. (It should be noted that because of the ionic strength of these solutions, this value actually would relate to the activity of hydrogen ion rather than the concentration.) Thus, without having to readjust the parameters, the model correctly predicted the experimental results above about 0.6 V. Though it should be noted, that at pH values above 1 (not shown), the polarization curves began to shift upward and no longer fit the model.

Similar work was also carried out using sulfuric acid. In this case the sulfate/bisulfate equilibrium added complexity both because of the changing ionic strength and changing relative amounts of various anions in the solutions. Two types of tests were conducted. One

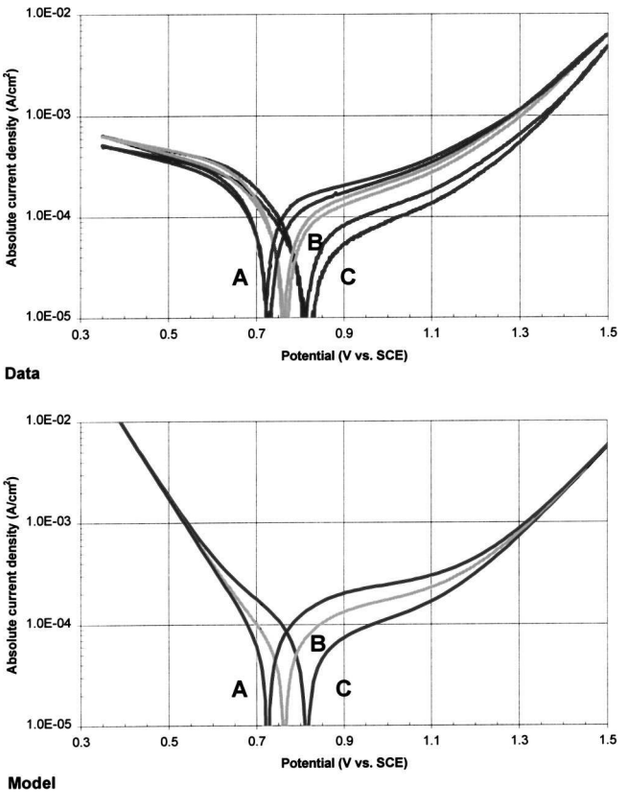

Figure 9. The effect of pH, showing data at three different pH values and the trends predicted for the three pH values using the modeled mechanism. Data measured at a graphite electrode, 4000 rpm, 2 M $HClO_4$ + $NaHCO_3$, 34 mM V(IV), and 16 mM V(V). (A) pH −0.50, (B) pH −0.04, and (C) pH 0.27.

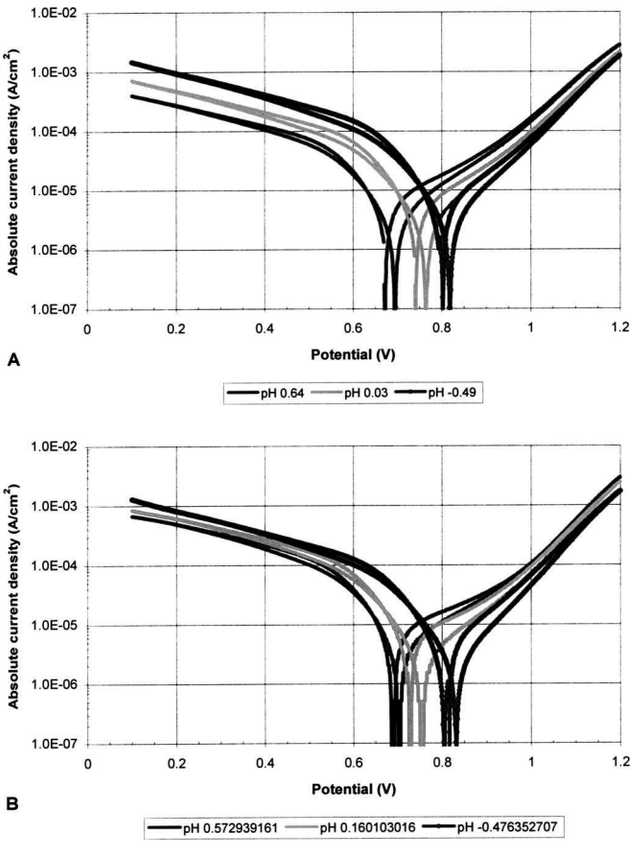

Figure 10. Polarization curves in different sulfuric acid electrolytes. (Measured at a graphite electrode, 4000 rpm, and 0.2 mV/s.) (A) 33 mM V(IV) and 14 mM V(V), H_2SO4/K_2SO_4 buffer (2 M total sulfate). (B) 31 mM V(IV) and 16 mM V(V), 2, 0.5, and 0.2 M H_2SO_4 solutions.

test started with 2 M H_2SO_4, which was step wise neutralized with $NaHCO_3$ (hence closer to constant ionic strength), and the other started with 0.05 M H_2SO_4 to which acid was added. The results are shown in Fig. 10A and B. Several differences from the results with perchlorate were noted. The currents near the reversible potential were much lower, while those in the anodic Tafel region were higher, thus requiring an adjustment in the scan limits to see the regions of interest. Between the two set of data in sulfate solutions, the results with constant sulfate + bisulfate (Fig. 10A) had a dependence on pH of the currents in the cathodic region, which is not apparent in Fig. 9A nor Fig. 10B. This indicates that the amounts of sulfate and bisulfate present may also have an influence.

The effect of total vanadium concentration is shown in Fig. 11. The observed currents increased proportionally with the concentration as would be expected for a first order reaction. It is interesting to note the general shape of the curves remains the same, thus all parts of the curves including the shoulder increase by the same proportion. The effect of changing the ratio of VO^{2+} to VO_2^+ is shown in Fig. 12. Model fits are also shown. One set of kinetic parameters was used and the three curves were then generated by changing the entered vanadium concentrations. While not providing a perfect fit, the model does however correctly predict the observed trends.

One problem with the model is its inability to predict the very unusual Tafel slope in the cathodic region (about 400-500 mV/decade). Even if an unusually low symmetry factor is used for the path 3 ECC step, the model will then not correctly fit in the area near the reversible potential. The unusual Tafel slope does, however, appear to be related to the path 3 ECC step. This is because path 2 would predict a horizontal plateau (see Fig. 8B) with a linear pH dependence. However, the high Tafel slope region is relatively pH independent (no apparent dependence in Fig. 9A and Fig. 10B and roughly a 0.5 power dependence in Fig. 10A). It is also interesting that when examining the model diagrammed in Fig. 7, the product

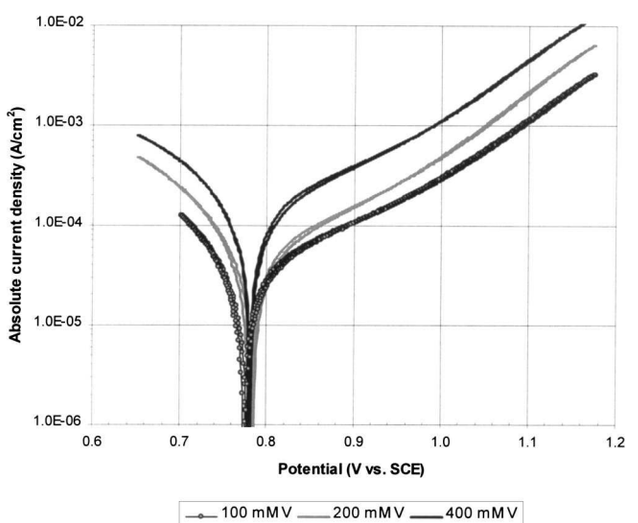

Figure 11. Polarization curves at various vanadium concentrations. Graphite electrode, 4000 rpm, 0.1 mV/s, 1 M H_2SO_4. 100 mM is *ca.* 55 mM V(IV) and 45 mM V(V), 200 mM is *ca.* 110 mM V(IV) and 90 mM V(V), and 400 mM is *ca.* 250 mM V(IV) and 150 mM V(V).

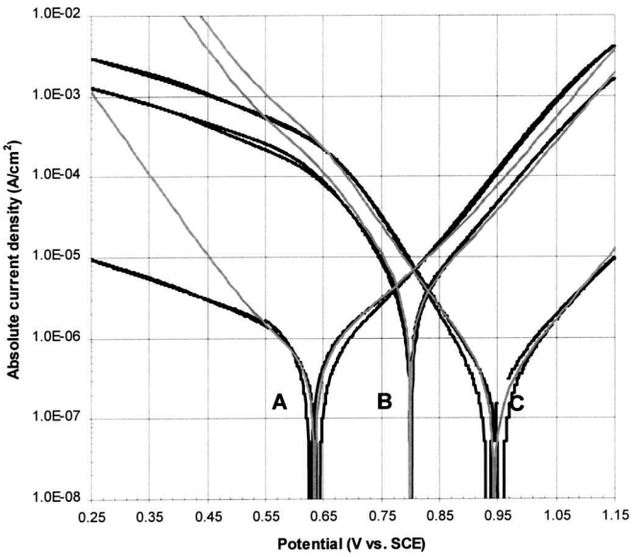

Figure 12. Data (in black) and predicted curves using the modeled mechanism (gray) for different ratios of V(IV) to V(V). Graphite electrode, 6000 rpm, 0.2 mV/s, 1 M H_2SO_4. (A) *ca.* 49.9 mM V(IV) and 0.1 mM V(V), (B) 25 mM V(IV) and 25 mM V(V), (C) *ca.* 0.2 mM V(IV) and 49.8 mM V(V).

of the path 3 ECC step is written as $VO_2 \cdot 4\ H_2O$. Being a neutral species, it might be expected to precipitate and possibly foul the electrode if the concentration of this intermediate exceeds its solubility. Pourbaix lists this species in solid form as V_2O_4.[14] Thus, an unusual Tafel slope in this region of the polarization curve is not actually inconsistent with the model. However, more work is required to understand the true cause of the unusual Tafel slope at higher overvoltages in the cathodic region, as other factors may also need to be considered.

Thus, a model based on the mechanism, as described in Fig. 7, appears to correctly predict the trends in the measured data. This is a very good result considering that the model is relatively simple, only including the range of possible elementary reaction steps between vanadyl (VO^{2+}) and vanadic (VO_2^+). It should be noted that previous workers have noted unusual shoulders in the polarization curves for the VO^{2+}/VO_2^+ redox reaction. The shoulders have been suggested to be due to sulfate complexes, carbon surface group interactions, and $VO^{2+} - VO_3^-$ complexes.[16,33] However, we have shown that much of the unusual polarization curve responses can be explained on the basis of the normally expected mechanistic pathways for the reactions. This explanation also fits the data quite well in both sulfuric acid and perchloric acid and over a range of VO^{2+} to VO_2^+ ratios (which would be difficult based on the other suggested explanations). Thus it is hoped that this improved description of the redox system mechanism will be useful for improved modeling and optimization of vanadium redox flow battery systems.

It is also felt, however, that the other suggested influences on the reactions are important for completely understanding the reactions. For example, sulfate complexes are likely the cause of the differences between Fig. 10A and B. And such complexes, as well as mixed vanadium complexes, likely become more important at higher vanadium and sulfuric acid concentrations. Finally, the role of surface oxide groups on carbon electrodes is often considered important for electron transfer, especially for the redox reactions of noncomplexed transition metal ions.[34,35] Variations in the rates of the VO^{2+}/VO_2^+ redox reaction, depending on the type of carbon used and its method of preparation, have been reported[16-18] and indicate the sensitivity of the reaction to the carbon surface. Thus a complete understanding of the reactions should also take into account the role of surface carbon groups as catalytic sites including possible adsorption and desorption steps. The role of surface sites may also be important for understanding the unusual Tafel slope for the reduction of VO_2^+ at higher cathodic overpotentials. The competitive and possibly potential dependent adsorptions of VO_2^+ and VO^{2+} may lead to a complex potential dependence of the reaction rate. Also, as mentioned above, blocking of the reaction sites on the carbon surface by a slowly desorbing or slowly dissolving species (such as a VO_2-type compound), might also affect the apparent Tafel slope.

Conclusions

The mechanism of the redox reactions between vanadyl (VO^{2+}) and vanadic (VO_2^+) were investigated. A model was developed based on the various possible steps in the overall reaction as shown in Fig. 7. The model could be used to fit the observed data over a range of pH, concentrations, and ratios of species. The results of the fit are consistent with a mechanistic path that changes depending on the overpotential.

The unusual Tafel slope at higher overpotential for the reduction of VO_2^+ of 400 to 500 mV/decade could not be directly explained by the model, though it could be related to a $VO_2 \cdot 4\ H_2O$ (or equivalent) intermediate species. However, while the model can clarify the underlying steps of the redox reactions, other aspects related to the role of carbon surface sites and solution complexes, need to be further investigated in order to completely understand the system.

Acknowledgments

The authors thank Dr. S. Miyake and Professor M. Skyllas-Kazacos for useful discussions, and Colin Stewart for carrying out some additional tests to help complete this paper.

The National Research Council of Canada assisted in meeting the publication costs of this article.

References

1. R. J. Remick and P. G. P. Ang, U.S. Pat. 4,485,154 (Nov 1984).
2. M. Skyllas-Kazacos, M. Rychick, and R. Robins, U.S. Pat. 4,786,567 (Nov 1988).
3. *RETScreen International, Renewable Energy Project Analysis*, Software, CANMET Energy Diversification Research Laboratory, Natural Resources Canada, http://retscreen.gc.ca/
4. J. Hawkins and T. Robbins, in *Proceedings of the 21st International Telecommunications Energy Conference, INTELEC 99*, IEEE, paper 27-3 (1999).
5. J. Hawkins and T. Robbins, in *Proceedings of the 23rd International Telecommunications Energy Conference, INTELEC 01*, IEEE, p. 652-6 (2001).
6. R. L. Largent, M. Skylas-Kazacos, and J. Chieng, in *Proceedings of the 23rd Photovoltaic Specialists Conference*, IEEE, p. 1119 (1993).
7. Ch. Fabjan, J. Garche, B. Harrer, L. Jorissen, C. Kolbeck, F. Philippi, G. Tomazic, and F. Wagner, *Electrochim. Acta,* **47**, 825 (2001).
8. C. J. Rydh, *J. Power Sources,* **80**, 21 (1999).
9. S. Zhong, C. Padeste, M. Kazacos, and M. Skyllas-Kazacos, *J. Power Sources,* **45**, 29 (1993).
10. B. Sun and M. Skyllas-Kazacos, *Electrochim. Acta,* **37**, 1253 (1992).
11. B. Sun and M. Skyllas-Kazacos, *Electrochim. Acta,* **37**, 2459 (1992).
12. M. Shimada, Y. Iizuka, and T. Hukazu, U.S. Pat. 4,496,637 (Jan 1985).
13. Y. Isreal and L. Meites, Vanadium, in *Encyclopaedia of Electrochemistry of the Elements*, Vol. VII, A. J. Bard, Editor, Chap. 2, p. 293, Marcel Dekker, New York (1976).
14. M. Pourbaix, *Atlas of Electrochemical Equilibria in Aqueous Solutions*, 2nd ed., p. 234, NACE, Houston, TX (1974).
15. F. J. Miller and H. E. Zittel, *J. Electroanal. Chem.,* **7**, 116 (1964).
16. S. Zhong and M. Skyllas-Kazacos, *J. Power Sources,* **39**, 1 (1992).
17. E. Sum, M. Rychcik, and M. Skyllas-Kazacos, *J. Power Sources,* **16**, 85 (1985).
18. M. Gattrell, J. Park, B. MacDougall, S. McCarthy, and J. MacDonald, in *Vanadium—Geology, Processing and Applications*, M. F. Taner, P. A. Riveros, J. E. Dutrizac, M. A. Gattrell, and L. M. Perron, Editors, p. 79, Canadian Institute of Mining, Metallurgy and Petroleum, Montreal, Canada (2002).
19. *Technical Note 200—Potentiostat Stability Considerations*, EG&G Princeton Applied Research, Princeton, NJ.
20. I.-F. Hu, D. H. Karweik, and T. Kuwana, *J. Electroanal. Chem.,* **188**, 59 (1985).
21. *CRC Handbook of Chemistry and Physics*, D. R. Lide, Editor, CRC Press, Boca Raton, FL (1999).
22. R. L. McCreery, *Electroanalytical Chemistry*, A. J. Bard, Editor, Vol. 17, p. 221, Marcel Dekker, New York (1991).
23. S. Miyake and N. Tokuda, in *Vanadium—Geology, Processing and Applications*, M. F. Taner, P. A. Riveros, J. E. Dutrizac, M. A. Gattrell, and L. M. Perron, Editors, p. 95, Canadian Institute of Mining, Metallurgy and Petroleum, Montreal, Canada (2002).

24. F. A. Cotton and G. Wilkinson, *Advanced Inorganic Chemistry*, 5th ed., p. 665, John Wiley & Sons, New York (1988).
25. C. F. Baes, Jr. and R. E. Mesmer, *The Hydrolysis of Cations*, p. 197, John Wiley & Sons, New York (1976).
26. P. Blanc, C. Madic, and J. P. Launay, *Inorg. Chem.,* **21**, 2923 (1982).
27. N. Kausar, R. Howe, and M. Skyllas-Kazacos, *J. Appl. Electrochem.,* **31**, 1327 (2001).
28. X. Lu, *Electrochim. Acta,* **46**, 4281 (2001).
29. A. A. Ivakin and E. M. Voronova, *Russ. J. Inorg. Chem.,* **18**, 956 (1973).
30. S. Uchiyama, K. Nozaki, A. Negishi, K. Kato, H. Kaneko, and M. Kobayashi, Abstract 1C03, the 42nd Battery Symposium in Japan Abstracts, The Electrochemical Society of Japan, p. 348 (2001).
31. A. J. Bard and L. R. Faulkner, *Electrochemical Methods*, p. 442, John Wiley & Sons, New York (1980).
32. J. Koutecky and R. Brdicka, *Collect. Czech. Chem. Commun.,* **12**, 337 (1947).
33. F. Z. Dzhabarov and S. V. Gorbachev, *Russ. J. Phys. Chem.,* **38**, 729 (1964).
34. P. Chen, M. A. Fryling, and R. McCreery, *Anal. Chem.,* **67**, 3115 (1995).
35. C. A. McDermott, K. R. Kneten, and R. L. McCreery, *J. Electrochem. Soc.,* **140**, 2593 (1993).